Gonzalo R. Arce, David J. Brady, Lawrence Carin, Henry Arguello, and David S. Kittle

Compressive Coded Aperture Spectral Imaging

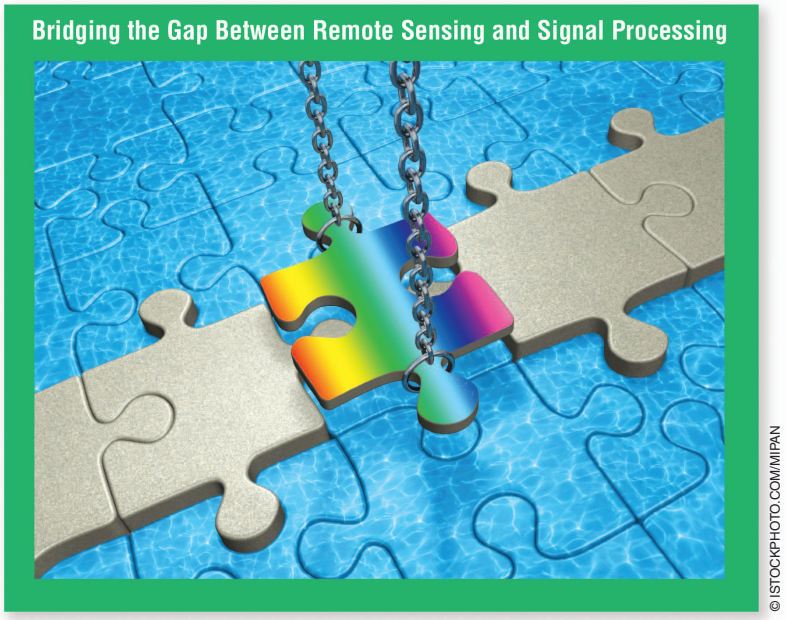

An introduction

Imaging spectroscopy involves the sensing of a large amount of spatial information across a multitude of wavelengths. Conventional approaches to hyperspectral sensing scan adjacent zones of the underlying spectral scene and merge the results to construct a spectral data cube. Push broom spectral imaging sensors, for instance, capture a spectral cube with one focal plane array (FPA) measurement per spatial line of the scene [1], [2]. Spectrometers based on optical bandpass filters sequentially scan the scene by tuning the bandpass filters in steps. The disadvantage of these techniques is that they require scanning a number of zones linearly in proportion to the desired spatial and spectral resolution. This article surveys compressive coded aperture spectral imagers, also known as *coded aperture snapshot spectral imagers* (*CASSI*) [1], [3], [4], which naturally embody the principles of compressive sensing (CS) [5], [6]. The remarkable advantage of CASSI is that the entire data cube is sensed with just a few FPA measurements and, in some cases, with as little as a single FPA shot.

Digital Object Identifier 10.1109/MSP.2013.2278763
Date of publication: 5 December 2013

INTRODUCTION

CS dictates that one can recover spectral scenes from far fewer measurements than that required by conventional linear scanning spectral sensors. To make this possible, CS relies on two principles: sparsity, which characterizes the spectral scenes of interest, and incoherence, which shapes the sensing structure [5], [7]. Sparsity indicates that spectral images found in nature can be concisely represented in some basis Ψ with just a small

number of coefficients. This is indeed the case in spectral imaging where natural scenes exhibit correlation among adjacent pixels and also across spectral bands [2]. Incoherence refers to the structure of the sampling waveforms used in CS that, unlike the signals of interest, have a dense representation in the basis Ψ [7]. The remarkable discovery behind CS is that it is possible to design sensing protocols capable of capturing the essential information content in sparse signals with just a small number of compressive measurements. The sensing modality simply correlates incoming signals with a small number of fixed waveforms that satisfy the incoherence principle. The signals of interest are then accurately reconstructed from the small number of compressive measurements by numerical optimization [5], [6], [8]–[11]. In CASSI, the random projections occur naturally as the result of the optical dispersion phenomena affecting coded aperture light fields as they transverse a prism before these are integrated by the imaging detector.

Our intent in this article is to overview the fundamental optical phenomena behind compressive spectral imaging sensors, present the key mathematical concepts embodying the sensing and reconstruction mechanisms, and describe the optimization framework used to design optimal coded apertures in a number of applications, including hyperspectral image reconstruction, spectral selectivity, and superresolution. The article describes many practical aspects of the instrumentation, including calibration, discretization models, parameter design, and physical limitations, and it illustrates results with real data and imagery. A fascinating aspect of compressive spectral sensing is that it draws from various disciplines within optics, signal processing, and probability theory. Our survey is to highlight the rich interaction among these fields of study as they come together in the discovery of novel compressive spectral sensors. Our treatment explains as plainly as possible four fundamental aspects of CASSI:

1) the sensing problem
2) coded aperture optimization
3) reconstruction algorithms
4) computational spectral imaging.

It should be noted that compressive spectral imaging is of interest in many fields and advances in this area are growing rapidly. Consequently, it is not possible to review all work in the field, and we focus on CASSI type compressive optical sensing. The topics in this tutorial are complemented by a companion article in this issue [12], where other approaches and methods are described.

THE SPECTRAL SENSING PROBLEM

The sensing physical phenomena in CASSI is strikingly simple, yet it adheres to the incoherence principles required in CS. In its simplest form, CASSI measurements are realized optically by a coded aperture, a dispersive element such as a prism, and an FPA detector [1], [3]. The coding is applied to the (spatial-spectral) image source density $f_0(x; y; \lambda)$ by means of a coded aperture $T(x; y)$ as realized by the CASSI system depicted in Figure 1, where $(x; y)$ are the spatial coordinates and λ is the wavelength [3]. The resulting coded field $f_1(x; y; \lambda)$ is subsequently modified by a dispersive element before it impinges onto the FPA detector. The compressive measurements across the FPA are realized by the integration of the dispersed field $f_2(x; y; \lambda)$ over the detector's spectral range sensitivity.

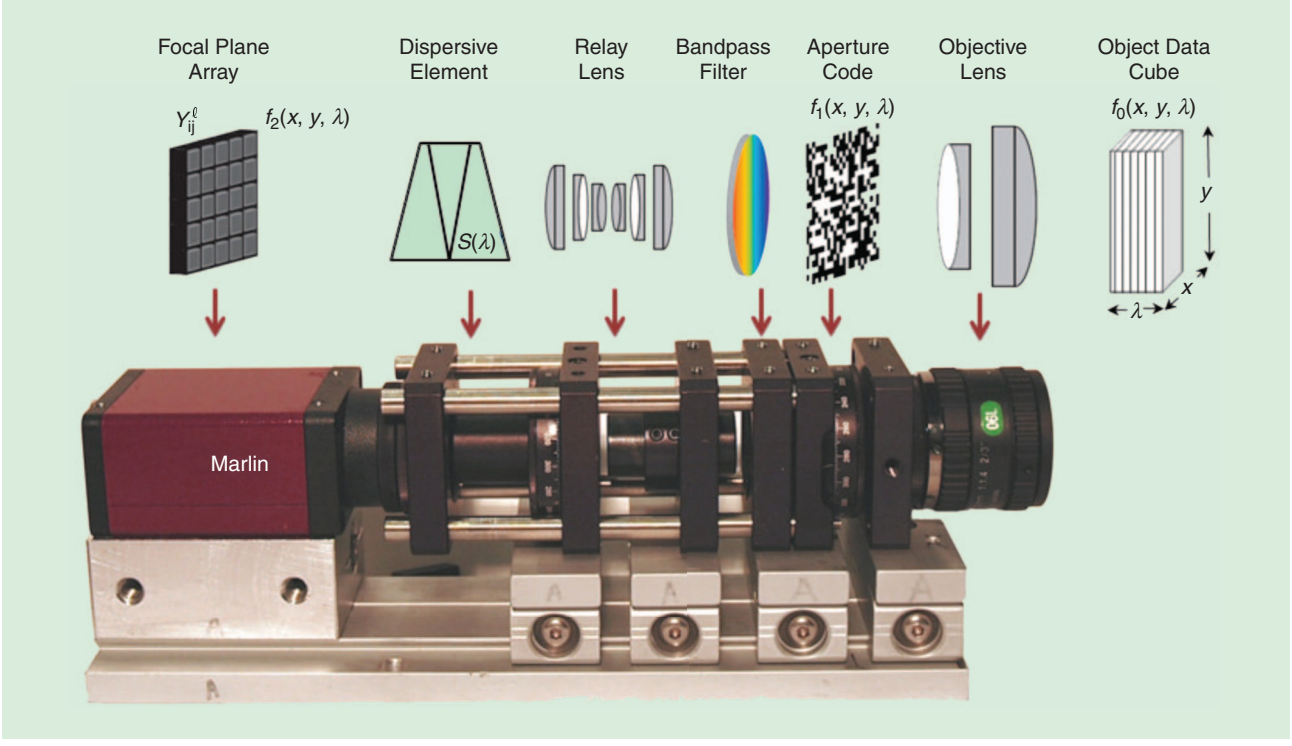

[FIG1] Compressive CASSI sensor components. (Image courtesy of David J. Brady and David S. Kittle.)

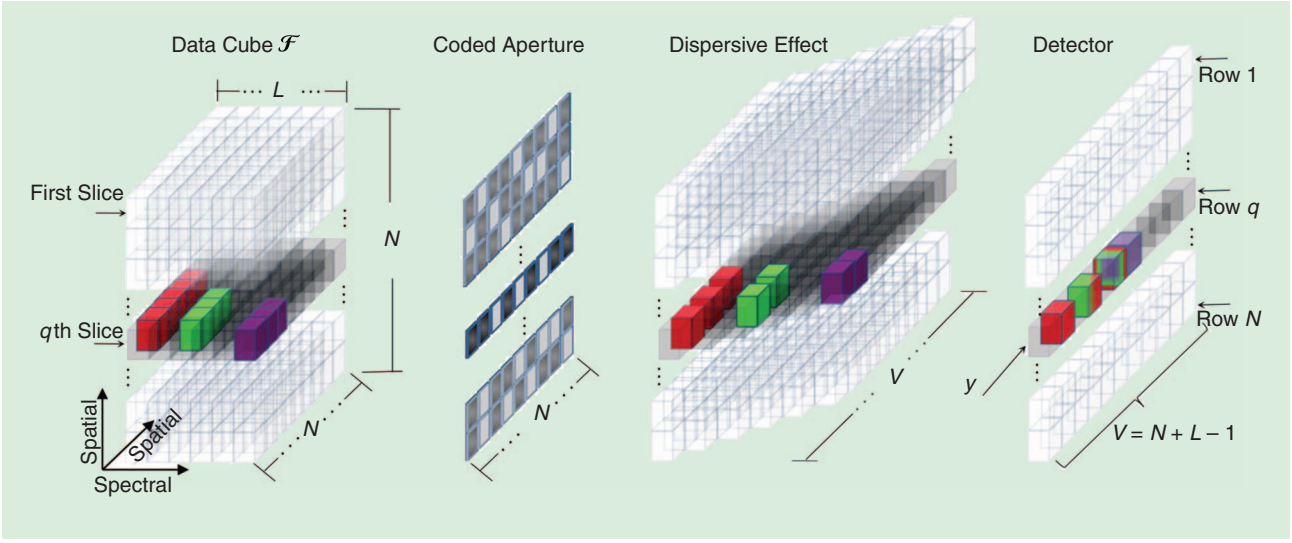

[FIG2] An illustration of the spectral optical flow in CASSI. The qth slice of the data cube $\mathcal{F}$ with 11 nonzero voxels is coded by a row of the coded aperture and dispersed by the prism. The detector captures the intensity y by integrating the coded light.

The sensing mechanism is illustrated by the discretized model shown in Figure 2, where the spectral data cube $\mathcal{F}$ having L spectral bands and $N \times N$ spatial pixels is first amplitude modulated by a pixelated $N \times N$ coded aperture $\mathbf{T}$.

In this case, $\mathbf{T}$ is a *block*- or *unblock*-coded aperture such that the energy along the spectral coordinate of the data cube is punched out when a block-coded aperture element is encountered. As the coded field transverses the prism, it is then spatially sheared along one spatial axis. In essence, each coded image plane at a fixed wavelength is shifted along the x-axis where the amount of shifting increases with the wavelength coordinate index. Finally, the coded and dispersed field is "collapsed" in the spectral dimension by the integration of the energy impinging on each detector element over its spectral range sensitivity. The integrated field is then measured by the FPA detector elements.

Several properties of the sensing phenomena model should be pointed out [13], [14]. First, note that the $N \times N$ spatial dimensions of the spectral data cube are mapped to an array of $V \times N$ FPA measurements, where $V = N + L - 1$. This is due to the dispersion of the optical field as it transverses the prism. Second, observe that the optical coding across rows of the FPA measurements are mutually independent. That is, the aperture coding affecting one row slice of the data cube is independent from the coding affecting other row slices in the data cube. These characteristics of the sensing phenomena are important, as they shape subsequent signal processing algorithms. Third, note how the sequence of optical transformations altogether end up in a set of compressive linear measurements in the FPA detector. As Figure 2 illustrates, each FPA shot captures a massive set of compressive measurements.

The discretized output at the detector can thus be modeled as [3]

$$Y_{j\ell} = \sum_{k=0}^{L-1} \mathcal{F}_{j(\ell+k)(k)}\, T_{j(\ell+k)} + \omega_{j\ell}, \tag{1}$$

where $Y_{j\ell}$ is the intensity measured at the j, ℓ position of the detector whose dimensions are $N \times (N + L - 1)$, L is the number of spectral bands, $T_{j\ell}$ is the binary coded aperture, and $\omega_{j\ell}$ is the noise of the system. In essence, (1) sums each of the spectral image slices that have been coded and spatially shifted in proportion to the wavelength index k. Notice in (1) that each discrete spectral band is defined such that a continuous region of the analog spectrum span one pixel in the detector.

Assume that the bandpass filter of the instrument limits the spectral components between λ_1 and λ_2. If the pixel width of the detector and of the coded aperture are both equal to Δ, then the number of resolvable bands L is limited by $L = \alpha((\lambda_2 - \lambda_1)/(\Delta))$, where for a given wavelength λ, $\alpha\lambda$ corresponds to the dispersion induced by the prism, i.e., to the displacement of light in the focal plane along the x-axis.

The spectral resolution is limited by Δ/α. The horizontal and vertical spatial resolutions are limited by Δ, and the number of spatially resolvable pixels of the underlying scene is $N \times N$.

For spectrally rich scenes or very detailed spatial scenes, a single-shot FPA measurement is not sufficient, and additional shots are required, each with a distinct coded aperture that remains fixed during the integration time of the detector. Time-varying coded apertures can be realized by a spatial light modulator or by a lithographic mask actioned by a piezoelectric device [4], [15], [16]. It was also shown in [15] and [16] that the ensemble of say, $K << L$ FPA shots in one-dimensional vectorized form $\mathbf{y} = [\mathbf{y}_0^T, \ldots, \mathbf{y}_{K-1}^T]^T$, can be rewritten in the standard form of an underdetermined system of linear equations

$$\mathbf{y} = \mathbf{A}\boldsymbol{\theta} = \mathbf{H}\boldsymbol{\Psi}\boldsymbol{\theta} + \boldsymbol{\omega}, \tag{2}$$

where $\mathbf{A} = \mathbf{H}\boldsymbol{\Psi} \in \mathbb{R}^{KN^2 \times LN^2}$ is the CASSI sensing matrix, $\boldsymbol{\theta}$ is a sparse representation of the data cube in a three-dimensional (3-D) basis $\boldsymbol{\Psi}$, and $\boldsymbol{\omega}$ represents the noise of the system. A

Kronecker basis $\Psi = \Psi_1 \otimes \Psi_2$ is often used, where Ψ_1 is the two-dimensional-wavelet Symmlet-8 basis and Ψ_2 is the cosine basis [17]. The matrix $\mathbf{H}$ in (2) accounts for the effects of the coded aperture and the prism. The sensing matrix $\mathbf{A}$ thus couples $\mathbf{H}$ with the representation basis $\boldsymbol{\Psi}$. The coded aperture is considered binary, and the dispersive element is considered linear. In practice, it is necessary to take into account the various optical artifacts and nonideal characteristic of the optical system. Furthermore, the underlying principles of CASSI described above are general and are thus, in principle, applicable to imaging with FPAs sensitive to any region of the visible and infrared (IR) radiation of the electromagnetic spectrum.

Signal recovery in CASSI entails solving an underdetermined linear system of equations. Given the set of measurements $\mathbf{y}$, the inverse CS problem consists on recovering $\boldsymbol{\theta}$ such that the $\ell_2 - \ell_1$ cost function is minimized

$$\arg\min_{\boldsymbol{\theta}} ||\,\mathbf{y} - \mathbf{A}\boldsymbol{\theta}\,||^2 + \lambda\,||\,\boldsymbol{\theta}\,||_1, \tag{3}$$

where λ is a regularization constant. The inverse problem in (3) will be addressed next. At this point, however, it should be emphasized that the sensing matrix $\mathbf{A}$ will play a pivotal role in sensing and thus its design is of key importance. Other cost functions could be used instead of (3). For example, an approach based on the stable recovery of a low-rank and joint-sparse matrix can be used to reconstruct the hyperspectral information. In this case, the optimization problem is regularized to minimize jointly a nuclear norm and a $\ell_2 - \ell_1$ norm [18].

To illustrate the underlying concepts above, a wide spectral bandwidth reconstruction is shown in Figure 3, acquired with a recently developed UV-visible CASSI instrument [19]. The object was illuminated using SoLux daylight emulation bulbs and bandpass filtered by a Baader Planetarium (Germany) UV-IR cut filter with transmission from 420 to 680 nm. A random, binary coded aperture was used in the instrument with a minimum feature size of two pixels and total area on the detector of $1,988 \times 1,988$ pixels. Figure 3 shows the comparison between a snapshot reconstruction and a multishot reconstruction with 24 frames. The prism dispersion is nonlinear, where the shorter wavelengths disperse significantly more than longer wavelengths. This yields higher spectral resolution and lower spatial resolution in the shorter wavelengths and corresponding higher spatial resolution and lower spectral resolution for longer wavelengths, shown in the blue spectral channel in Figure 3(a) and the red spectral channel in (b), respectively.

Code features fewer than two pixels place high demands on the optics, alignment, and calibration of the CASSI instrument, especially for small pixel size detectors. The coded aperture is required to disambiguate the spatial and spectral information that is multiplexed at the detector. For smaller code features, the optical blur, forward model, calibration, detector noise, and pixel sampling of the code have a larger impact on the reconstruction. A code feature size of two pixels (total area of four pixels) guarantees that regardless of where the feature is sampled on the detector, it will cover at least one pixel to fully modulate the signal. Smaller features will generally modulate less, where the worst case scenario involves a one-pixel feature sampled by four pixels, reducing the modulation to 25%. In general, sampling a square wave (in our case, the coded aperture) requires infinite sample points. Even a sine wave would require at least two pixels assuming spatial Nyquist sampling and interpolation under the assumption of lowpass filtering. At the limits of small code features, adequate models [14] are required to compensate for undersampling the coded aperture.

A calibration process is realized in CASSI in which the spectral channels are determined so that the centers of each channel, at the finest scale, are separated by one column of detector pixels. Thus, the position of a channel corresponds to a fixed

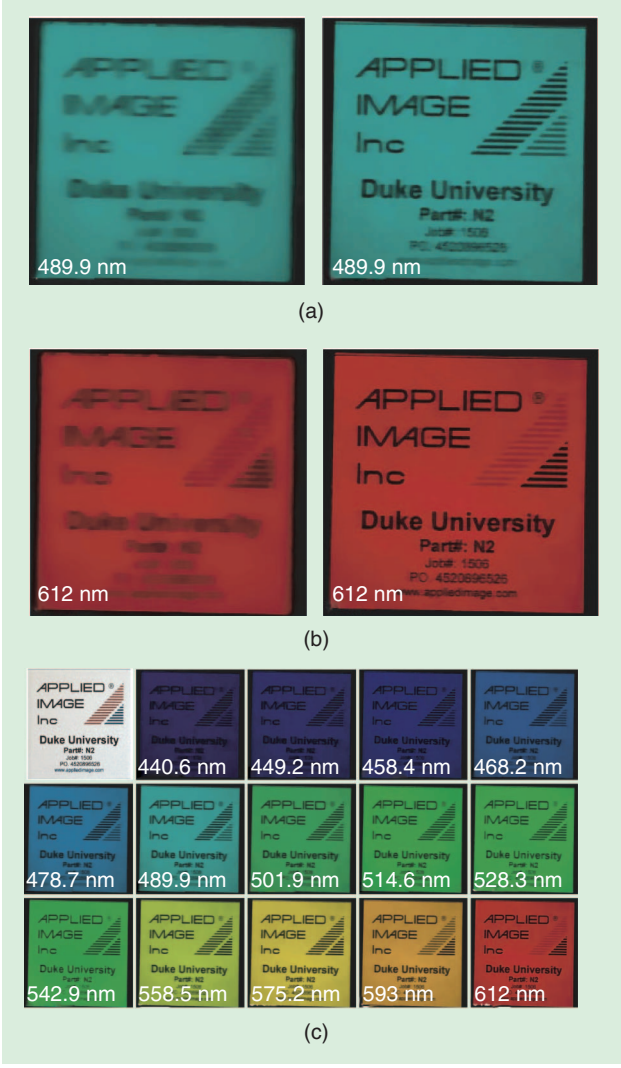

[FIG3] A comparison between snapshot and multishot CASSI reconstructions: (a) snapshot, 490 nm and 24-frame reconstruction at 490 nm, (b) snapshot, 612 nm and a 24-frame reconstruction at 612 nm, and (c) selected wavelengths from the 24-frame, reconstructed data cube. An RGB image of the object taken with an SLR digital camera is shown in the upper left part of (c). Notice the relative spatial resolution for the blue and red spectral channels.

dispersion in terms of detector pixels relative to a fixed spectral channel. Charge-coupled device (CCD) measurements at equally spaced wavelengths are taken after uniformly illuminating the coded aperture with monochromatic wavelength of light within the bandpass of the system. These calibration measurements are used to build a modified system operator that accounts for the optical blur and nonlinear dispersion. The set of measurements is obtained with careful efforts to reduce or remove certain data corruptive processes, including the dark noise on the CCD, the nonuniform spectral intensity of the calibrating light source, and the nonuniform spectral sensitivity of the CCD. An alternative calibration procedure can be realized using specifically designed coded apertures for calibration and by using a high-order model of the CASSI phenomena [14].

CODED APERTURE OPTIMIZATION

The sensing matrix $\mathbf{A}$ in (1) plays a crucial role in the mathematics of the inverse CS problem. A large body of literature in CS specifically deals with characterizing the "goodness" of $\mathbf{A}$ [5], [6]. In CASSI, $\mathbf{A}$ is determined by the matrix $\mathbf{H}$, which can be shown to have the structure shown in Figure 4 [4], [15], [16]. It consists of a set of diagonal patterns (circled) that repeat in the horizontal direction, each time with a unit downward shift, as many times as the number of spectral channels. Each diagonal pattern, circled in Figure 4, is the coded aperture pattern itself. Just below, the next set of diagonal patterns are determined by the coded aperture pattern used in the next FPA shot. The matrix $\mathbf{H}$ will thus have as many sets of diagonal patterns as FPA measurements. Initially, commonly used coded apertures in CASSI included Hadamard matrices, S matrices, and Bernoulli random matrices [1].

The use of these coded apertures was principally motivated by the realization that they are well conditioned when used in least square estimation [1]. However, these code designs do not fully exploit the rich theory of CS. Given that the coded apertures determine the nonzero entries of the sensing matrix, the important question can be asked: Can the coded apertures be optimally designed? Remarkably, the answer is yes, where the restricted isometry property (RIP) provides the optimization criteria [6].

The RIP establishes the conditions necessary for $\mathbf{A}$ such that the ℓ_2 norm of the underlying 3-D spectral image is approximately preserved under the transformation $\mathbf{A}\boldsymbol{\theta}$. More precisely, for each integer $S = 1, 2, \ldots$, define the restricted isometry constant δ_s of the matrix $\mathbf{A}$ as the smallest constant such that the RIP inequality $(1-\delta_s)\,||\boldsymbol{\theta}||_2^2 \le ||\mathbf{A}\boldsymbol{\theta}||_2^2 \le ||\boldsymbol{\theta}||_2^2(1+\delta_s)$ holds for all S-sparse vectors θ [7]. A more intuitive description of the RIP is that it requires that subsets of S columns taken from $\mathbf{A}$ to be nearly orthogonal, or equivalently, that all $m \times |\mathcal{T}|$ column submatrices $\mathbf{A}_{|\mathcal{T}|}$ of $\mathbf{A}$ are well conditioned for all $|\mathcal{T}| \le S$. This, in turn, implies that all pairwise distances between S-sparse vectors are well preserved in the compressed signal space such that $(1-\delta_{2s})\,||\boldsymbol{\theta}_1 - \boldsymbol{\theta}_2||_2^2 \le ||\mathbf{A}\boldsymbol{\theta}_1 - \mathbf{A}\boldsymbol{\theta}_2||_2^2 \le ||\boldsymbol{\theta}_1 - \boldsymbol{\theta}_2||_2^2(1+\delta_{2s})$ holds for all S-sparse vectors $\boldsymbol{\theta}_1$, $\boldsymbol{\theta}_2$. If the RIP holds for the sensing matrix $\mathbf{A}$, one can discriminate among S-sparse signals

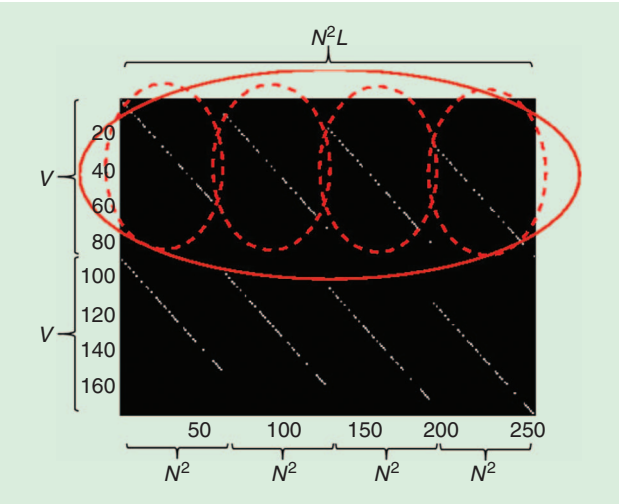

[FIG4] The sensing matrix $\mathbf{H}$ where the (circled) diagonal patterns repeating horizontally correspond to the coded aperture pattern used in the first FPA shot. The second coded aperture pattern determines the next set of diagonals. The figure depicts the sensing of four spectral bands and two FPA shots.

in the compressed domain and consequently it is then possible to accurately reconstruct any $\boldsymbol{\theta}$ from its projection $\mathbf{A}\boldsymbol{\theta}$.

The RIP inequality can be rewritten as $|\,||\mathbf{A}\boldsymbol{\theta}||_2^2 - ||\boldsymbol{\theta}||_2^2\,| \le \delta_s\,||\boldsymbol{\theta}||_2^2$ or equivalently as $|\langle (\mathbf{A}\mathbf{A}^T - \mathbf{I})\boldsymbol{\theta}, \boldsymbol{\theta}\rangle| \le \delta_s\,||\boldsymbol{\theta}||_2^2$, where $\mathbf{I}$ is an identity matrix. Constraining the vector $\boldsymbol{\theta}$ to $||\boldsymbol{\theta}||_2^2 = 1$, taking the supremum over all the vectors $\boldsymbol{\theta}$ with $\mathrm{supp}(\boldsymbol{\theta}) \subset \mathcal{T}$, $|\mathcal{T}| \le S$, and taking the maximum with respect to all the subsets $\mathcal{T}$ leads to $\lambda_s = \max_{\mathcal{T}\subset[n],|\mathcal{T}|\le s} \lambda_{\max}(\mathbf{A}_{|\mathcal{T}||\mathcal{T}|} - \mathbf{I}_{|\mathcal{T}|})$, where $\mathbf{A}_{|\mathcal{T}||\mathcal{T}|} = \mathbf{A}_{|\mathcal{T}|}^T\mathbf{A}_{|\mathcal{T}|}$, and $n = N^2L$. The probability of satisfying the RIP condition is thus calculated by estimating the statistical distribution of the maximum eigenvalue $\lambda_{\max}$ of the matrices $\mathbf{A}_{|\mathcal{T}||\mathcal{T}|} - \mathbf{I}_{|\mathcal{T}|}$.

The design strategy is then formulated as seeking the set of coded apertures $\{T_{j\ell}^0, \ldots, T_{j\ell}^{K-1}\}$, such that

$$T_{j\ell}^0, \ldots, T_{j\ell}^{K-1} = \underset{\{T_{j\ell}^0,\ldots,T_{j\ell}^{K-1}\}}{\mathrm{argmin}} \max_{\mathcal{T}\subset[n],|\mathcal{T}|\le S} \lambda_{\max}(\mathbf{A}_{|\mathcal{T}|}^T\mathbf{A}_{|\mathcal{T}|} - \mathbf{I}_{|\mathcal{T}|}), \quad (4)$$

where the entries of $\mathbf{A}_{|\mathcal{T}||\mathcal{T}|}$ are determined by the coded apertures. For a set of K coded apertures $\{T_{j\ell}^0, T_{j\ell}^1, \ldots, T_{j\ell}^{K-1}\}$, as depicted in Figure 5, it turns out that the correlation variable [Figure 5(b)]

$$z_{\ell_1\ell_2}^j = T_{j\ell_1}^0 T_{j\ell_2}^0 + T_{j\ell_1}^1 T_{j\ell_2}^1 + \cdots + T_{j\ell_1}^{K-1} T_{j\ell_2}^{K-1} \quad (5)$$

strongly influences (4) and consequently the RIP in CASSI [20]. As depicted in Figure 5, $T_{j\ell_1}^i T_{j\ell_2}^i$ is the product of two elements of the ith coded aperture, both at the jth row, but at the column positions ℓ_1 and ℓ_2. The first- and second-order statistics of $z_{\ell_1\ell_2}^j$, specifically the mean $E\{z_{\ell_1\ell_2}^j\} = m$ and $\mathrm{Var}(z_{\ell_1\ell_2}^j) = \sigma^2$, have a critical effect on (4). The expectation in this case is over the random selection of the entries $T_{j\ell_1}^i T_{j\ell_2}^i$.

Let the entries of $\boldsymbol{\Psi}$ be $\Psi_{j,k}$, then using the structure of the matrices $\mathbf{H}$ in Figure 4, the entries $(\mathbf{A}_{|\mathcal{T}||\mathcal{T}|})_{k_1k_2}$ can be obtained as [4]

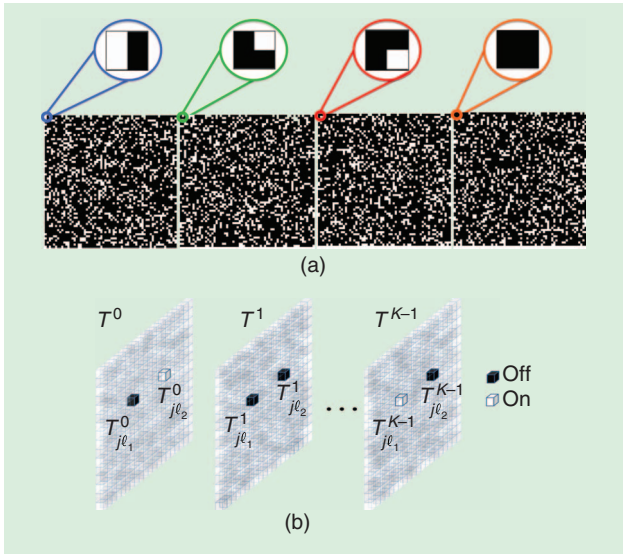

[FIG5] (a) An optimal ensemble of four 64×64 Boolean-coded apertures. White colored squares indicate $T^i_{j\ell} = 1$, and black colored squares indicate $T^i_{j\ell} = 0$. Zoomed-in areas show that each spatial coordinate in the ensemble contains only one one-valued entry. (b) The elements $T^k_{\ell_1(\ell_2-j_1)}$ and $T^k_{\ell_1(\ell_2-j_2)}$ for $k = 0, \ldots, K-1$ are multiplied and the products are then added to obtain one realization of the random variable z in (5).

$$\sum_{j_1=0}^{N-1} \sum_{j_2=0}^{N-1} \sum_{r_1=0}^{L-1} \sum_{r_2=0}^{L-1} z^{j_1}_{(j_2-r_1)(j_2-r_2)} \Psi_{\ell_{j_1 j_2 r_1}, \Omega_{k_1}} \Psi_{\ell_{j_1 j_2 r_2}, \Omega_{k_2}} \tag{6}$$

for $k_1, k_2 = 0, \ldots, |\mathcal{T}| - 1$, where Ω_{k_1} and $\Omega_{k_2} \in \mathcal{T}$. Note that the coded aperture entries determine $z^{j_1}_{(j_2-r_1)(j_2-r_2)}$ in (6), which in turn determine the statistical properties of the entries $(\mathbf{A}_{|\mathcal{T}||\mathcal{T}|})_{k_1 k_2}$. It was also shown in [20] that the entries in (6) can be roughly approximated as independent and identically distributed Gaussian variables $(\mathbf{A}_{|\mathcal{T}||\mathcal{T}|})_{k_1 k_2} \simeq \mathcal{N}(0, C_1(\sigma^2 + m^2))$ such that the concentration of measure for this type of matrices can be applied [21]. A relation between the statistics of (6) and the probability of correct reconstruction is then established using the concentration of measure. The variance of the entries in the Gaussian approximation depends on the variance σ^2 and mean m of the variables $z^i_{\ell_1 \ell_2}$. To guarantee that the diagonal elements of $\mathbf{A}_{|\mathcal{T}||\mathcal{T}|}$ satisfy $\mathrm{E}((\mathbf{A}_{|\mathcal{T}||\mathcal{T}|})_{k\,k}) = 1$ for all k, these are normalized by constraining the coded apertures to satisfy $\sum_{i=0}^{K-1} (T^i_{j\,\ell})^2 = C$ for all j and ℓ, where C is a selectable constant. The so-called *Boolean-coded apertures* are defined as those whose entries satisfy $T^i_{j\,\ell} \in \{0, 1\}$. In which case, $m = C^2/K^2$ and $\sigma^2 = (K-C)^2/\ (K^2(K-1))$. The term $m^2 + \sigma^2$ can be minimized by setting $C = 1$ implying that in each spatial position, only one coded aperture from the ensemble of K-codes contains a nonzero value. Thus, for each j and ℓ the optimal coded aperture entries under the criterion (4) are obtained by satisfying the constraints $T^{i_0}_{j\,\ell} = 1$ and $T^i_{j\,\ell} = 0$ for $i \neq i_0$.

Figure 5(a) illustrates an optimal Boolean ensemble for four coded apertures of size 64×64. As indicated in the zoomed-in regions of the coded apertures, there is only one nonzero element for each j, ℓ position of the ensemble. Figure 6(a) illustrates a portion of the ground truth of a 16-band spectral data cube sensed with a monochromator. Figure 6(b) illustrates a corresponding compressive measurement. Figure 6(c) shows the reconstruction of a data cube of 16 bands using the optimal Boolean-coded apertures. Figure 6(d) depicts the reconstruction using an ensemble with random entries. Notice in Figure 6 that the resulting spectral data cubes are shown as they would be viewed by a Stingray F-033C CCD color camera.

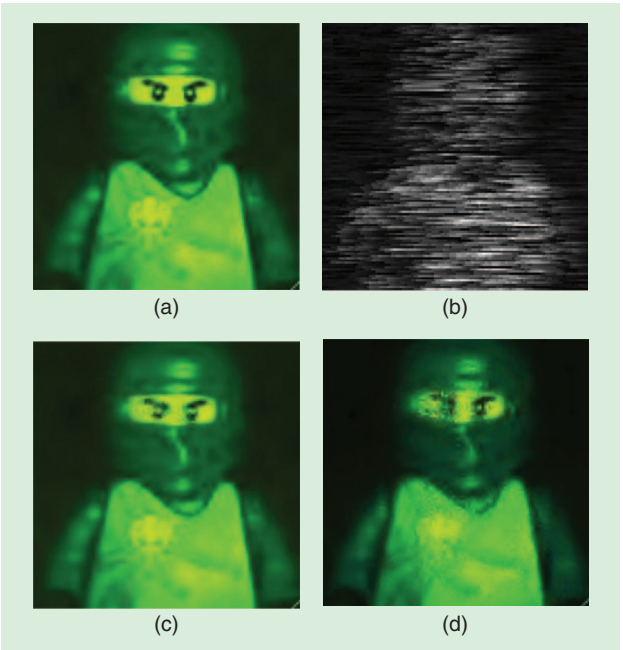

[FIG6] (a) The original data cube and (b) compressive FPA measurement. Reconstructions from six shots using (c) Boolean (PSNR 40.41 dB) and (d) random (PSNR 27.72 dB). The resulting spectral data cubes are shown as they would be viewed by a Stingray F-033C CCD color camera. (Image courtesy of G.R. Arce and H. Arguello.)

RECONSTRUCTION FROM COMPRESSED MEASUREMENTS

Several numerical algorithms are available to solve the inverse problem in (3). These can be grouped into one of five computational approaches [10]. Algorithms based on greedy pursuit iteratively find an estimate of the solution by selecting atoms of a dictionary and the correspondent weighting factors such that the signal can be represented as a linear combination of these vectors. This approach is implemented by algorithms such as the orthogonal matching pursuit (OMP) and compressive sampling matching pursuit (CoSaMP). The second type of algorithms solve a convex optimization problem. This includes interior-point methods such as ℓ_1-magic software and gradient-descent methods like the sparse reconstruction via separable approximation (SpaRSA), the two-step iterative shrinkage/thresholding algorithm (TwIST), and the gradient projections for sparse reconstruction algorithm (GPSR) [10], [22], [23]. The third approach uses a Bayesian framework that finds a maximum a posteriori estimator assuming a prior distribution of the unknown coefficients of the signal to recover [8]. Other techniques include

nonconvex optimization [24] and brute force, which attempts to find the solution by trying all possible support sets. A tutorial review of the algorithms in each of these class-types and their associated complexity is found in [10]. Typical computations performed by these algorithms include matrix pseudoinverses, sparse basis transformations, and vector-matrix multiplications. Given that the underlying signals are high dimensional, these calculations require a large number of floating point operations. For instance, in each iteration of the GPSR algorithm, approximately $O(KN^4L)$ operations are computed where K is the number of measurement shots, N is the spatial dimensions, and L is the number of spectral channels of the data cube. Reconstructions of large scenes are indeed overwhelming since they can take hours in desktop architectures [13], [16].

The computational burden can be ameliorated by working with separable sensing operators [25] or fast field-programmable gate array and graphics processing unit implementations of the reconstruction algorithms [26]. Instead of relying on hardware solutions, the computational complexity can be also addressed by exploiting the physical properties of the CASSI optical sensing phenomena. In particular, it is possible to reconstruct the underlying 3-D data cube from a set of reconstructions obtained from nonoverlapping FPA windowed measurements. In this manner, the GPSR reconstruction algorithm performs $O(KB^4L)$ operations per iteration on each $B\times B$ windowed measurement with $B^4 \ll N^4$. After the recovery of the set of images, these are tiled together to assemble the complete data cube reconstruction.

Consider a $B\times B$ measurement window $\mathbf{Y}^i_{m,n}$ within the FPA detector at the ith shot, as shown in Figure 7, where the energy in the windowed measurements is traced back through the optical system. After the prism, the energy to be collected by the $B\times B$ FPA window is a coded and dispersed square source cube with L spectral bands. If these voxels are traced back before they impinge on the prism and the coded aperture, the voxels no longer form a cube but instead they form an oblique parallelepiped consisting of L spectral bands, with each one shifted one spatial position in the horizontal axis. Figure 7 illustrates how an oblique parallelepiped $\mathbf{F}_{mn}$ of the data cube, which is amplitude modulated by a coded aperture of size $B\times(B+L-1)$ and spectrally sheared by the prism, results on a $B\times B$ block of measurements at the detector. In other words, the voxels that are sensed in a $B\times B$ area of the detector emanate from an oblique volume in the source and not from a cube. Furthermore, the oblique parallelepiped volume, once it is sheared by the prism, is transformed into a $B\times B$ cube before it impinges onto the detector.

The energy impinging on an adjacent nonoverlapping window at the FPA can be traced back to the source in a similar manner, such that the entire FPA measurement $\mathbf{Y}^i$ can be expressed as an ensemble of $B\times B$ nonoverlapping measurement windows as

$$\mathbf{Y}^i=\begin{bmatrix}\mathbf{Y}^i_{0,0} & \mathbf{Y}^i_{0,1} & \cdots & \mathbf{Y}^i_{0,V'-1}\\ \vdots & \vdots & \ddots & \vdots\\ \mathbf{Y}^i_{N'-1,0} & \mathbf{Y}^i_{N'-1,1} & \cdots & \mathbf{Y}^i_{N'-1,V'-1}\end{bmatrix}. \tag{7}$$

The total number of windows in the set is $N'V'$, with $N'=N/B$ and $V'=\lceil (N+L-1)/(B)\rceil$, with B determining the partition block size.

Now consider the reconstruction of the oblique parallelepiped based on its compressive projections $\mathbf{Y}^i_{m,n}$. The compressive projection of the parallelepiped block $\mathbf{F}_{mn}$ is given by

$$\mathbf{y}^i_{mn}=\mathbf{H}^i_{mn}\,\mathbf{f}_{mn}+\boldsymbol{\omega}^i_{mn}, \tag{8}$$

where $\mathbf{H}^i_{mn}$ is a $B^2\times B^2L$ submatrix of $\mathbf{H}^i$ obtained by choosing the rows and columns that affect each windowed FPA measurement, $\mathbf{y}^i_{mn}$ and $\mathbf{f}_{mn}$ are the vectorized representations of $\mathbf{Y}^i_{m,n}$ and $\mathbf{F}_{mn}$, respectively. Equation (8) is referred to as the *block-model projection*. The set of windowed measurements from sequential FPA shots can then be assembled as in the CASSI model to obtain $\mathbf{y}_{mn}=[(\mathbf{y}^0_{mn})^T,\ldots,(\mathbf{y}^{K-1}_{mn})^T]^T$ and the correspondent matrices $\mathbf{H}^i_{mn}$ are assembled as $\mathbf{H}_{mn}=[(\mathbf{H}^0_{mn})^T,\ldots,(\mathbf{H}^{K-1}_{mn})^T]^T$. The matrices $\mathbf{H}^i_{mn}$ preserve the structure of $\mathbf{H}^i$ in Figure 4 except that the dimensions are now considerably smaller. The multishot block CASSI model can be rewritten as

$$\mathbf{y}_{mn}=\mathbf{H}_{mn}\,\mathbf{f}_{mn}+\boldsymbol{\omega}_{mn}. \tag{9}$$

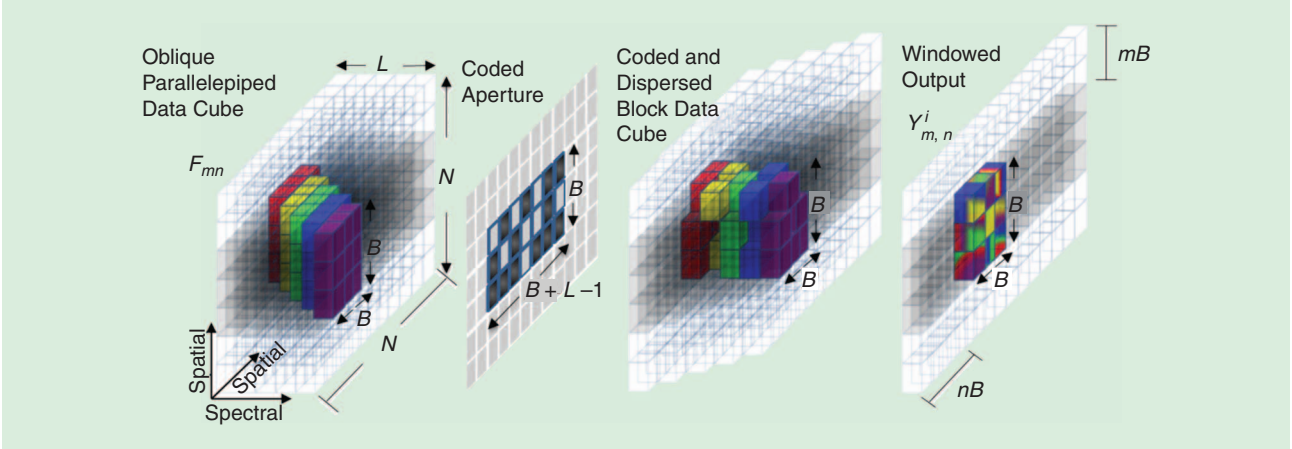

[FIG7] Each $B\times B$ window at the detector results from sensing a $B\times B\times L$ oblique parallelepiped block of the data cube. (Reprinted and used with permission from [13].)

Each individual set of windowed measurements $\mathbf{y}_{mn}$ in (9) is now used to recover an oblique parallelepiped $\hat{\mathbf{F}}_{mn}$ within the data cube. A vectorized representation of $\hat{\mathbf{F}}_{mn}$ is then recovered by solving

$$\hat{\mathbf{f}}_{mn} = \boldsymbol{\Psi}'\left(\underset{\boldsymbol{\theta}_{mn}}{\operatorname{argmin}} \|\mathbf{y}_{mn} - \mathbf{H}_{mn}\boldsymbol{\Psi}'\boldsymbol{\theta}'\|_2 + \tau\|\boldsymbol{\theta}_{mn}\|_1\right), \quad (10)$$

where $\boldsymbol{\theta}'$ is a sparse representation of $\hat{\mathbf{f}}_{mn}$ in the basis $\boldsymbol{\Psi}'$. Notice that the inverse problem in (10) is similar to that in (3) of the traditional approach. The difference lies in that the sparsifying basis $\boldsymbol{\Psi}'$ representing the Kronecker product of a wavelet basis and the cosine basis has smaller dimensions than $\boldsymbol{\Psi}$ since $\mathbf{F}_{mn}$ is a smaller section of the data cube $\mathbf{F}$.

The full data cube $\hat{\mathbf{F}}$ is assembled by tiling all the reconstructed oblique parallelepipeds. Since the number of operations per iteration in CS reconstruction algorithm grows rapidly with the size of the measurement vector, the computational complexity in the block CASSI model decreases rapidly as the number of partitions increase. In particular, the GPSR in CASSI performs approximately $O(KN^4L)$ operations per iteration to recover a $N \times N \times L$ data cube using K FPA measurements. The block model reduces the number of operations to $O(KN^2B^2L)$ operations. If distinct processors are used to reconstruct separately each of the N'^2 blocks, then the number of operations per core is $O(KB^4L)$.

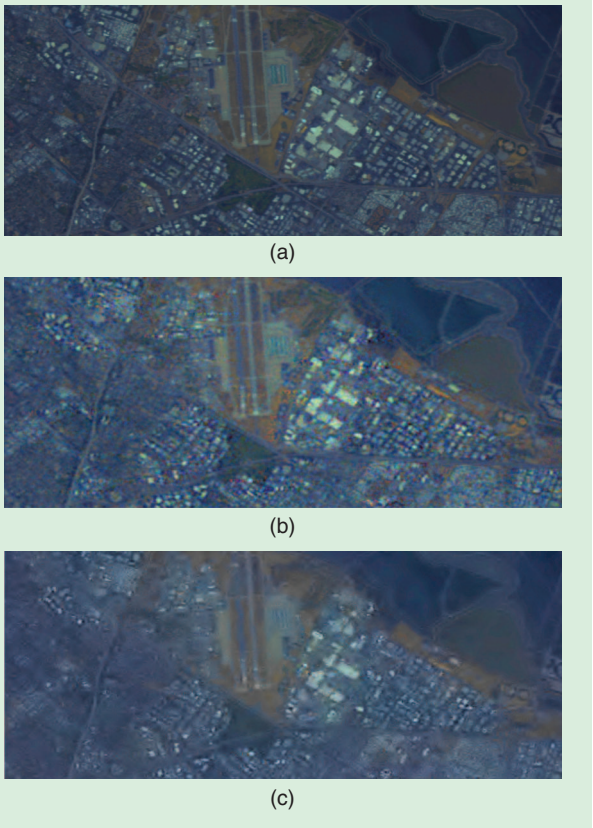

[FIG8] (a) The original RGB and zoomed-in version of the $512 \times 512 \times 32$ data cube. Reconstructions for 10 FPA measurement shots using (b) the block approach with block size $B = 64$, 31.84 dB and (c) the traditional reconstruction approach, 30.99 dB. Block overlapped was used in this example [13].

Figure 8 illustrates the reconstruction quality attained by the block CASSI model. A detailed analysis of the block CS performance in PSNR is presented in [13] where the improvements in image reconstruction are described at length. Figure 8 shows an original $512 \times 512 \times 32$ data cube, the block model reconstructed data cube, and the traditional CASSI model reconstruction. Using an Intel Core i7 3.30 GHz processor PC with 32 GB RAM memory, the block model and the standard CASSI take approximately $0.71K + 3.6$ min and $1.58K + 7.8$ min, respectively, to reconstruct the complete data cube, where K is the number of shots. The reconstruction of one parallelepiped associated with a single block takes $0.045K + 0.28$ min; thus, if multiple processing is available, the block reconstruction can offer significant faster processing.

The block CASSI model is general and can be used with any CS reconstruction algorithm. For instance, the Bayesian reconstruction framework introduced in [27] is noteworthy, with an approximate posterior distribution on model parameters inferred assuming a prior distribution of the unknown coefficients of the signal to recover. In this approach, one seeks to recover not only multiple $\mathbf{f}_{mn}$ but to also infer on the underlying dictionary with which the data may be represented. Specifically, we wish to jointly recover all $\{\mathbf{f}_{mn}\}$ and $\boldsymbol{\Psi}'$, where the latter is an overcomplete dictionary. It is assumed that $\mathbf{f}_{mn} = \boldsymbol{\Psi}'\boldsymbol{\theta}_{mn} + \boldsymbol{\omega}_{mn}$, where $\boldsymbol{\Psi}' \in \mathbb{R}^{B^2L \times U}$ with $U > B^2L$; $\boldsymbol{\theta}_{mn}$ is sparse, and $\boldsymbol{\omega}_{mn}$ again represents noise. Each measurement is of the form $\mathbf{y}_{mn} = \mathbf{H}_{mn}\boldsymbol{\Psi}'\boldsymbol{\theta}_{mn} + \boldsymbol{\omega}_{mn}$. The theoretical underpinnings are developed in [28], where a number of illustrative experiments are given. A key distinction of this approach with conventional CS reconstruction algorithms is that $\boldsymbol{\Psi}'$ and $\boldsymbol{\theta}_{mn}$ are estimated simultaneously, implying that the measurements are "blind" to the underlying $\boldsymbol{\Psi}$ in which each $\mathbf{f}_{mn}$ may be sparsely rendered. This is achievable because $N'V'$ different signals $\mathbf{y}_{mn}$ are jointly processed and analyzed. This framework has been coined as *blind* CS [28]. In this framework, a prior is placed on the noise variance, and this is inferred within the analysis. The noise statistics are assumed Gaussian within the prior, but the posterior may differ from the Gaussian assumption. The dictionary learning employed here represents each patch of data in terms of a sparse subset of dictionary elements. One may show that this model has close similarities to Gaussian mixture modeling (GMM) with (near) low-rank covariance matrices [29], with this in turn closely related to recent work on low-rank data modeling [30]. Low-rank models assume the data live in a single linear subspace, with the GMM assume the data live in a union of linear subspaces [29].

COMPUTATIONAL SPECTRAL IMAGING

The coded aperture patterns determine the quality of CASSI measurements. Good codes provide better measurements that, in turn, render more accurate signal reconstructions. Computational spectral imaging goes a step further by jointly optimizing the coded apertures and the computational modules to produce new types of imagery that could benefit vision in

different applications. This tutorial describes computational algorithms for spectral selectivity and super resolution. Computational tools exist for a number of other applications as detailed in the recent literature [1], [31], [36], [37] and in the companion article [12] in this issue.

SPECTRAL SELECTIVITY

It is often known a priori that objects of interest in a scene do not contain a spectral component over the full range of wavelengths but in a subset of wavelengths. Notably, the coded aperture patterns can be designed so as to maximize the information content on a prespecified subset of spectral bands of particular interest. Spectral selectivity is of interest in many applications, including wide-area airborne surveillance, remote sensing, and tissue spectroscopy in medicine. The optimal spectral bands in airborne surveillance, for instance, depend on atmospheric conditions, time of day, the targets of interest, and the background against which the targets are viewed [4], [15]. Efforts placed on acquiring the entire spectral image cube, to then throw away a large portion of this data is wasteful in many regards.

To this end, coded apertures can be used to attain spectrally selective compressive measurements [4], [15]. A spectrally selective coded aperture, denoted as $\mathbf{T}^i$, is formed from two concatenated coded apertures, which simplifies the optimization. The first coded aperture $\mathbf{w}^i$ is a structured code optimized to attain the spectral band selectivity. The second coded aperture $\mathbf{r}^i$ is a pseudorandom binary code necessary to attain randomized measurements in CASSI. The coded aperture used in each measurement is obtained by the Hadamard product $\mathbf{T}^i = \mathbf{w}^i \circ \mathbf{r}^i$, and its optimization is divided in two parts. Since row measurements in CASSI are independently coded, the model in (2) is first rewritten as $\mathbf{y} = \sum_{k=0}^{V-1} \mathbf{H}'_k \mathbf{C} (\boldsymbol{\Theta}^T)^{k+1} \mathbf{w}$, where $\mathbf{y}$ is the compressive measurement and $\mathbf{H}'_k$ representing a row of the data cube $\mathbf{F}$ and the prism effect, $\mathbf{C}$ is an antidiagonal matrix with all the nonzero entries equal to one, and $\boldsymbol{\Theta}$ is a permutation matrix [4]. Note that the term $\mathbf{C}(\boldsymbol{\Theta}^T)^{k+1}\mathbf{w}$ represents the effects of the coded aperture operations on the sheared data cube $\mathbf{H}'_k$. Since the desired spectral bands of interest are known a priori, an approach to design the coded apertures is to create a desired compressive measurement $\mathbf{d}$ where the data cube is first modified such that the spectral bands that are of no interest are zeroed out. A compressive measurement based on the modified data cube would be ideal in the sense that it would only contain information from the spectral bands of interest. The desired compressive measurement is then obtained as $\mathbf{d} = \sum_{K=0}^{V-1} \mathbf{H}'_k \boldsymbol{\lambda}$ where the entries of $\boldsymbol{\lambda}$ are $\lambda_j = 1$ if the jth band is desired and zero elsewhere. The desired compressive measurement $\mathbf{d}$ is next equated to the compressive measurement $\mathbf{y}$ attained with the full data cube sensed by the CASSI imager leading to the following structures for the coded apertures

$$\mathbf{w}^j = (\boldsymbol{\Theta})^{j+1}\mathbf{C}^{-1}\boldsymbol{\lambda} \qquad j = 0, \ldots, L-1. \tag{11}$$

The solution in (11) requires L vectors, however, the number of vectors can be reduced by exploiting their interdependence. More specifically, to estimate $K < L$ linearly independent weight vectors, the coded apertures are arranged into the matrix $\mathbf{M}_w = [\mathbf{w}^0, \ldots, \mathbf{w}^{L-1}]$. The minimum number of shots K for a given set of bands of interest is the number of independent column K of $\mathbf{M}_w$ determined by $K = \text{rank}(\mathbf{M}_w)$, the rank of the matrix $\mathbf{M}_w$ [4]. The K linear independent columns of $\mathbf{M}_w$ are the linear independent weight vectors $\boldsymbol{\mathcal{W}} = [\mathbf{w}^{\alpha_0}, \ldots, \mathbf{w}^{\alpha_{K-1}}]$ selected from $\mathbf{M}_w$. The remaining $L-K$ columns of $\mathbf{M}_w$ can be estimated using the ensemble of vectors in $\boldsymbol{\mathcal{W}}$.

Once the components $\mathbf{w}^j$ of the coded apertures have been optimized, these are fixed and the companion pseudorandom components $\mathbf{r}^i$ are then optimized so as to further minimize the required number of shots. This is achieved by minimizing the rank of the matrix $\mathbf{M}_t = [\mathbf{r}^0 \ldots \mathbf{r}^{K-1}] \circ \boldsymbol{\mathcal{W}}$ such that $\text{rank}(\mathbf{M}_t) < \text{rank}(\mathbf{M}_w)$, where $\circ$ is the element by element multiplication operator and where the search of the vectors $\mathbf{r}^i$ is such that the CASSI measurements better satisfy the RIP. The rank minimization of $\mathbf{M}_t$ is an NP hard problem such that a stochastic algorithm can be used to approximately solve this optimization [4].

To illustrate the design of coded apertures with spectral selectivity, consider again the data cube $\mathcal{F}$ with 512×512 pixels of spatial resolution and $L = 24$ spectral bands ranging from 460 nm to 668 nm. The desired spectral bands are set to $\boldsymbol{\lambda} = [461\,\text{nm} - 479\,\text{nm}, 641\,\text{nm} - 668\,\text{nm}]$ as depicted in Figure 9(e). In this case, the initial rank of the matrix $\mathbf{M}_t$ is 24. Using a stochastic based optimization algorithm [4], the rank of the matrix $\mathbf{M}_t$ is minimized to 12. The resulting spectral data cubes are shown as they would be viewed by a Stingray F-033C CCD color camera: Figure 9(a) shows the original bands, Figure 9(b) depicts the reconstruction of the same scene from 12 Bernoulli random coded aperture compressive measurements, Figure 9(c) shows the results when 12 optimized coded apertures are used in the sensing and reconstruction, and Figure 9(d) shows one of the optimal spectrally selective coded apertures. Figure 9 illustrates the gain attained by optimal coded apertures in terms of spectral resolution and higher quality of reconstruction.

SUPERRESOLUTION

While FPAs are available across the IR spectrum, there is continued interest in the development of larger format FPAs for increased resolution [32], [33]. Increasing the size and resolution of FPAs comes with ever-increasing costs. Notably, coded apertures can be designed to yield superresolved reconstruction by leveraging computational imaging [34], [35]. The goal is to translate high-resolution scenes into compressed signals measured by low-resolution or small-format detectors. Superresolution can be attained not only spatially but also spectrally, where the number of spectrally resolved image planes is increased.

Let Δ_c and Δ be the coded aperture pitch and FPA pitch, respectively, and let $r = \Delta/\Delta_c$. A critical requirement to achieve superresolution is that $\Delta_c < \Delta$. If $\Delta = \Delta_c$, the resultant spectral imaging system is equivalent to the standard CASSI architecture. On the other hand, when the pitch resolution of the coded aperture is reduced to the extreme where all the elements

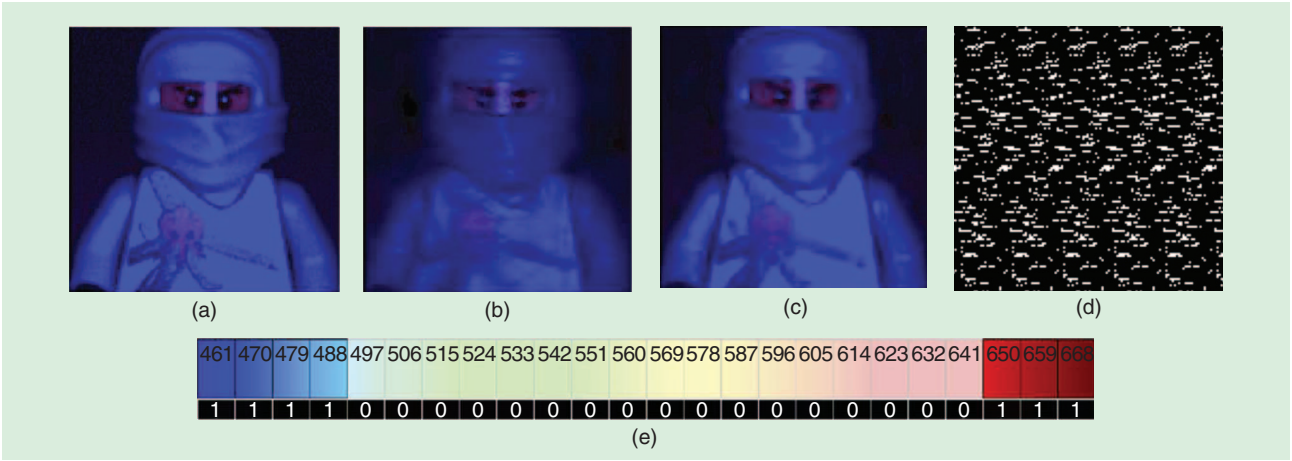

[FIG9] **The resulting spectral data cubes are shown as they would be viewed by a Stingray F-033C CCD color camera. (a) The original desired bands. Reconstructed images with 12 shots using (b) random codes (26.92 dB) and (c) optimized codes (31.02 dB). (d) An optimal coded aperture is illustrated. (e) Wavelengths of desired bands. (Reprinted and used with permission from [4].)**

of the coded aperture are mapped to just one pixel in the detector ($\Delta = N\Delta_c$), the imaging system becomes the single pixel camera [12]. Superresolution CASSI is realized when the pitch resolution lies somewhere between these two extremes, i.e., when Δ_c lies in the interval $((\Delta/N), \Delta)$. It is important to observe that the minimum value for Δ_c is limited by the diffraction limit of the instrument.

The random projections in superresolution CASSI are given by $\mathbf{y} = \mathbf{DH\Psi}\theta$, where $\mathbf{H}$ is the CASSI measurement matrix shown in Figure 4, and $\mathbf{D}$ is a decimation matrix with size $(N(N+L-1))/(r) \times N(N+L-1)$, where r represents the decimation ratio induced by the low-resolution FPA [35]. The decimation matrix $\mathbf{D}$ accounts for the integration of light in the detector when pixel mismatch $\Delta_c < \Delta$ is introduced. A set of K low-resolution FPA measurements are first captured, each one having $N' \times M'$ compressed measurements, with $N' = N/\Delta$ and $M = \lceil (M+L-1)/\Delta \rceil$ being the low-resolution detector height and width, respectively. Superresolution CASSI allows one to exploit subpixel information of a scene to obtain a high-resolution spectral image from low-resolution measurements. As the number of FPA measurement increases, the superresolved measurements lead to a rapid increase of image reconstruction quality. The standard CASSI measurements, on the other hand, cannot provide improved performance after a few shots. Figure 10 illustrates this concept for $r = 4$, where the CASSI image reconstruction quality after 48 shots (24.95 dB) is compared with the superresolved CASSI, which attains over a 3 dB gain in PSNR by exploiting subpixel information.

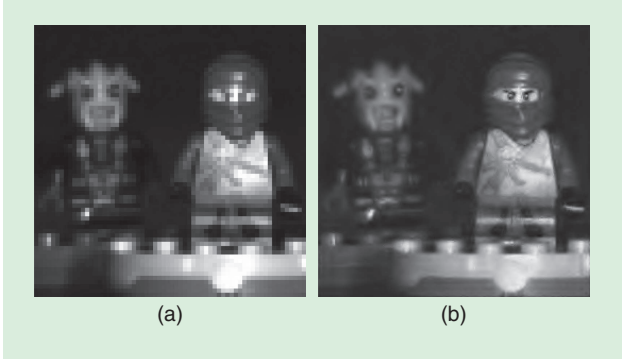

[FIG10] **(a) CASSI reconstruction (PSNR 24.95 dB) versus (b) superresolution CASSI reconstruction (PSNR 29.31 dB) for the sixth spectral band. In both cases 48 shots are used. (Images courtesy G.R. Arce and H. Arguello.)**

CONCLUSIONS

Compressive spectral imaging with coded apertures benefits from the use of simple optical sensing elements to harness compressive projections. CASSI snapshot spectral imagers are both, remarkably simple and surprisingly efficient, making them attractive in a number of applications in remote sensing and surveillance. Their power emerges from the combination of optics with the rich theories of CS and computational imaging. While CASSI spectral imagers naturally embody the congruence of these fields, new spectral imagers as well as more general multidimensional imaging sensors are being discovered by the use of more advanced optical and photonic devices as sensor elements. The potential of coded aperture optimization and optical sensing in multimode and multidimensional imaging holds great promise in the near future, providing fertile ground for signal processing exploration.

ACKNOWLEDGMENTS

This research was supported in part by the Office of Naval Research under contract NOOO14-1O-C-0 199, by the National Science Foundation under grants EECS-0725422 and CCF-0915800, and by the Air Force Office for Scientific Research under grant FA9550-11-1-0194.

AUTHORS

Gonzalo R. Arce (arce@udel.edu) is the Charles Black Evans Professor of electrical and computer engineering at the University of Delaware, Newark. He received the Ph.D. degree in

electrical engineering from Purdue University. He was the 2010 Fulbright–Nokia Distinguished Chair in information and communications technologies. His research interests include statistical signal processing and computational imaging, and he is a coauthor of several books in these areas. He was an associate editor and guest editor of several journals of the IEEE, Optical Society of America (OSA), and International Society for Optics and Photonics (SPIE). He is an IEEE Fellow.

David J. Brady (dbrady@duke.edu) leads the Duke Imaging and Spectroscopy Program (DISP), which builds computational imaging systems. His current DISP projects focus on snapshot gigapixel photography using multiscale optics, X-ray scatter tomography, millimeter wave diffraction tomography, focal tomography, and compressive spectral imaging. He is a Fellow of the IEEE, OSA, and SPIE.

Lawrence Carin (lcarin@ece.duke.edu) earned the Ph.D. degree in electrical engineering at the University of Maryland in 1989. Since 1995, he has been with the Electrical Engineering Department at Duke University, where he is now the William H. Younger Distinguished Professor. He was an associate editor of several journals of the IEEE and the Society for Industrial and Applied Mathematics. He is an IEEE Fellow.

Henry Arguello (henarfu@uis.edu.co) is an associate professor in the Department of Systems Engineering at Universidad Industrial de Santander, Colombia. He received the Ph.D. degree in 2013 from the Department of Electrical and Computer Engineering at the University of Delaware, Newark. His research interests include high-dimensional signal coding and processing, optical imaging, CS, hyperspectral imaging, optical code design, and computational imaging.

David S. Kittle (dsk12@duke.edu) earned the Ph.D. degree in electrical and computer engineering at Duke University in May 2013. He received the B.S. degree in electrical engineering in 2005 from Walla College in College Place, Washington. His research interests lie in computational imaging systems design, testing, and validation.

REFERENCES

[1] D. J. Brady, *Optical Imaging and Spectroscopy*. Hoboken, NJ: Wiley, 2009.

[2] M. Eismann, *Hyperspectral Remote Sensing*. Bellingham, WA: SPIE, 2012.

[3] A. A. Wagadarikar, R. John, R. Willett, and D. Brady, "Single disperser design for coded aperture snapshot spectral imaging," *Appl. Opt.*, vol. 47, pp. B44–B51, Apr. 2008.

[4] H. Arguello and G. R. Arce, "Rank minimization code aperture design for spectrally selective compressive imaging," *IEEE Trans. Image Processing*, vol. 22, no. 3, pp. 941–954, 2013.

[5] D. L. Donoho, "Compressed sensing," *IEEE Trans. Inform. Theory*, vol. 52, pp. 1289–1306, Apr. 2006.

[6] E. Candès, J. Romberg, and T. Tao, "Robust uncertainty principles: Exact signal reconstruction from highly incomplete frequency information," *IEEE Trans. Inform. Theory*, vol. 52, no. 2, pp. 489–509, 2006.

[7] E. J. Candès and M. B. Wakin, "An introduction to compressive sampling," *IEEE Signal Processing Mag.*, vol. 25, no. 2, pp. 21–30, Mar. 2008.

[8] J. Shihao, X. Ya, and L. Carin, "Bayesian compressive sensing," *IEEE Trans. Signal Processing*, vol. 56, no. 6, pp. 2346–2356, 2008.

[9] J. L. Paredes and G. R. Arce, "Compressive sensing signal reconstruction by weighted median regression estimates," *IEEE Trans. Signal Processing*, vol. 59, no. 6, pp. 2585–2601, June 2011.

[10] J. Tropp and S. Wright, "Computational methods for sparse solution of linear inverse problems," *Proc. IEEE*, vol. 98, no. 6, pp. 948–958, June 2010.

[11] M. Figueiredo, R. Nowak, and S. Wright, "Gradient projection for sparse reconstruction: Application to compressed sensing and other inverse problems," *IEEE J. Select. Topics Signal Processing*, vol. 1, no. 4, pp. 586–597, Dec. 2007.

[12] R. M. Willett, M. F. Duarte, M. A. Davenport, and R. G. Baraniuk, "Sparsity and structure in hyperspectral imaging," *IEEE Signal Processing Mag.*, vol. 31, no. 1, pp. 116–126, Jan. 2013.

[13] H. Arguello, C. V. Correa, and G. R. Arce, "Fast lapped block reconstructions in compressive spectral imaging," *Appl. Opt.*, vol. 52, no. 10, pp. D32–D45, 2013.

[14] H. Arguello, H. Rueda, Y. Wu, D. W. Prather, and G. R. Arce, "Higher-order computational model for coded aperture spectral imaging," *Appl. Opt.*, vol. 52, no. 10, pp. D12–D21, 2013.

[15] H. Arguello and G. R. Arce, "Code aperture optimization for spectrally agile compressive imaging," *J. Opt. Soc. Amer. A*, Opt. Image Sci., vol. 28, no. 11, pp. 2400–2413, Nov. 2011.

[16] D. Kittle, K. Choi, A. A. Wagadarikar, and D. J. Brady, "Multiframe image estimation for coded aperture snapshot spectral imagers," *Appl. Opt.*, vol. 49, no. 36, pp. 6824–6833, Dec. 2010.

[17] M. F. Duarte and R. G. Baraniuk, "Kronecker compressive sensing," *IEEE Trans. Image Processing*, vol. 21, no. 2, pp. 494–504, 2012.

[18] M. Golbabaee and P. Vandergheynst., "Compressed sensing of simultaneous low-rank and joint-sparse matrices," submitted for publication.

[19] D. S. Kittle, D. L. Marks, and D. J. Brady, "Design and fabrication of an ultraviolet-visible coded aperture snapshot spectral imager," *Opt. Eng.*, vol. 51, no. 7, pp. 071403–1–071403–10, 2012.

[20] H. Arguello and G. R. Arce, "Restricted isometry property in coded aperture compressive spectral imaging," in *2012 IEEE SSP Workshop*, Aug., pp. 716–719.

[21] M. Ledoux, *The Concentration of Measure Phenomenon*. Providence, RI: American Mathematical Society, 2001.

[22] M. Figueiredo, R. D. Nowak, and S. J. Wright, "Gradient projection for sparse reconstruction: Application to compressed sensing and other inverse problems," *IEEE J.* Select. *Topics Signal Processing*, vol. 1, no. 4, pp. 586–597, 2007.

[23] J. Bioucas-Dias and M. Figueiredo, "Alternating direction algorithms for constrained sparse regression: Application to hyperspectral unmixing," in *2010 2nd Workshop on Hyperspectral Image and Signal Processing: Evolution in Remote Sensing (WHISPERS),* pp. 1–4.

[24] R. Chartrand, "Exact reconstruction of sparse signals via nonconvex minimization," *IEEE Signal Processing Lett.*, vol. 14, no. 10, pp. 707–710, Oct. 2007.

[25] Y. Rivensons and A. Stern, "Compressed imaging with a separable sensing operator," *IEEE Signal Processing Lett.*, vol. 16, no. 6, pp. 449–452, 2009.

[26] Y. Fang, L. Chen, J. Wu, and B. Huang, "GPU implementation of orthogonal matching pursuit for compressive sensing," *2011 IEEE 17th Int. Conf. Parallel and Distributed Systems (ICPADS)*, pp. 1044–1047.

[27] A. Rajwade, D. Kittle, T.-H. Tsai, D. Brady, and L. Carin, "Coded hyperspectral imaging and blind compressive sensing," *SIAM J. Imaging Sci.*, vol. 6, no. 2, pp. 782–812, 2013.

[28] J. Silva, M. Chen, Y. Eldar, G. Sapiro, and L. Carin, "Blind compressed sensing over a structured union of subspaces," *IEEE Trans. Signal Processing*, submitted for publication.

[29] J. M. Duarte-Carvajalino, G. Yu, L. Carin, and G. Sapiro, "Task-driven adaptive statistical compressive sensing of gaussian mixture models," *IEEE Trans. Signal Processing*, vol. 61, no. 3, pp. 585–600, 2013.

[30] E. E. Candès and B. Recht, "Exact matrix completion via convex optimization," *Found. Comput. Math.*, vol. 9, no. 6, pp. 717–772, 2009.

[31] A. Ramirez, H. Arguello, G. R. Arce, and B. M. Sadler, "Spectral image classification from optimal coded-aperture compressive measurements," *IEEE Trans. Geosci. Remote Sensing*, to be published. DOI: 10.1109/TGRS.2013.2272378

[32] K. Krapels, R. Driggers, E. Jacobs, S. Burks, and S. Young, "Characteristics of infrared imaging systems that benefit from superresolution reconstruction," *Appl. Opt.*, vol. 46, no. 21, pp. 4594–4603, July 2007.

[33] A. Rogalski, *Fundamentals of Infrared Detector Technologies,* 2nd ed. Boca Raton, FL: CRC Press, 2011.

[34] R. Willett, R. Marcia, and J. Nichols, "Compressed sensing for practical optical imaging systems: A tutorial," *Opt. Eng.*, vol. 50, no. 7, pp. 072601–072601-13, July 2011.

[35] H. Arguello, H. Rueda, and G. R. Arce, "Spatial super-resolution in code aperture spectral imaging," in *SPIE Conf. Defense, Security and Sensing*, Baltimore, MD, Apr. 2012, pp. 83650A–83650A-6.

[36] A. Ramirez, G. R. Arce, and B. M. Sadler, "Compressive spectral image classification using redundant dictionaries," *IEEE Trans. Geosci. Remote Sensing*, submitted for publication.

[37] A. Ramirez, G. R. Arce, and B. M. Sadler, "Spectral image unmixing from optical coded-aperture compressive measurements," *IEEE Trans. Geosci. Remote Sensing*, submitted for publication.

[SP]